ANALYSIS OF MECHANOCHEMICAL DIFFUSION COUPLING PROCESSES BASED ON TRANSIENT CONTINUUM CHEMO-MECHANICAL COUPLING THEORY

Pengfei YU*, Wenchao SUN, Yaohong SUO, Yihan WU

 $School\ of\ Mechanical\ Engineering\ and\ Automation,\ Fuzhou\ University,\ Fuzhou,\ China\\ *corresponding\ author,\ yupengfei0422@fzu.edu.cn$

Chemical diffusion is vital in materials science and energy technology. Current Fick and non-Fick theories overlook the transient nature of diffusion. By referring to biomechanical axioms, we incorporate the transient expansion process and introduce characteristic time. This paper explores chemo-mechanical coupling in a spherical structure via transient continuum theory. The results show characteristic time changes in the diffusion equation from parabolic to hyperbolic, yielding finite diffusion speed and wave-like behavior, offering a basis for optimizing systems like lithium-ion batteries

Keywords: mechano-diffusion coupling; transient diffusion; characteristic time.



Articles in JTAM are published under Creative Commons Attribution 4.0 International. Unported License https://creativecommons.org/licenses/by/4.0/deed.en. By submitting an article for publication, the authors consent to the grant of the said license.

1. Introduction

Chemical diffusion refers to the directional migration of atoms or molecules of a substance due to the presence of a chemical potential gradient. In a system, when the chemical potential varies in different regions, the substance will diffuse from the region with a higher chemical potential to that with a lower chemical potential, aiming to achieve chemical potential equilibrium. As this phenomenon is ubiquitous in almost all materials and fields, the study of chemical diffusion in objects has always attracted extensive interest among researchers (Dai & Xiao, 2021; Hu et al., 2020). The study of this phenomenon has traditionally been based on Fourier's law of heat conduction and Fick's law of diffusion. Both of these laws assume that the propagation speed is infinite. Transient phenomena occurring under high temperatures or extremely large diffusion fluxes, accompanied by mass and heat transfer during chemical reactions, may lead to errors that contradict physical observations. Therefore, it is necessary to discuss the transient effects at finite speeds.

The research on non-Fourier heat conduction has inspired the study of non-Fick diffusion. In light of the analogous nature of heat conduction and mass diffusion, Dong and Jiang (1995) conducted an analysis of the physical process underlying diffusion mass transfer. They introduced the concept of mass propagation speed and formulated the diffusion differential equation for scenarios where the mass propagation speed is finite. This equation addresses the non-Fick diffusion mechanism, which deviates from the traditional Fick diffusion model, and provides a framework for understanding diffusion processes with finite propagation speeds, thereby enhancing the realism of the model in the context of mass transfer phenomena. Liu (2007) employed the least square method and Laplace transform to prognosticate the characteristic time of sodium chloride diffusion in aqueous solutions. This approach was facilitated by leveraging historical experimental data pertaining to the concentration of NaCl diffusion in water. Through computational analysis, Liu successfully obtained theoretical values that were in concordance

with the experimental data, thereby validating the finite propagation speed model for diffusion processes. Kuang (2014) integrated the generalized inertial entropy theory into the framework of continuum thermodynamics, thereby establishing a comprehensive theoretical model. This model elucidates that both heat and diffusion waves propagate at a finite speed, a departure from the infinite propagation speed implied by classical Fourier's law. Suo and Shen (2013a) employed the method of separation of variables to derive the double Fourier series solution for two-dimensional non-Fick diffusion, accommodating arbitrary initial and periodic boundary conditions. This theoretical framework was subsequently validated against both simulation and experimental results, demonstrating a heightened congruence with experimental data when utilizing non-Fick diffusion models. This finding underscores the superiority of non-Fick diffusion models in accurately capturing the complexities of mass transfer phenomena, particularly in scenarios where traditional Fick models fall short.

Diffusion processes are also indeed intricately linked with various physical phenomena, including stress or deformation fields (Yan et al., 2024), temperature fields (Nguyen et al., 2019), chemical reactions (Chen et al., 2023), and electric fields (Yu et al., 2016; Yu & Shen, 2014). This coupling is not merely coincidental but reflects the multifaceted nature of transport phenomena in materials science and engineering. Chu and Lee (1994) have indeed conducted research on the effect of stress on chemical diffusion, emphasizing the intricate relationship between mechanical stress and mass transport phenomena. Their work contributes to the understanding of how chemical stresses can influence diffusion processes, a topic of significant importance in materials science and engineering. Building upon the foundation of irreversible thermodynamics, inertial entropy, and inertial concentration, Hu and Shen (2013) have proposed variational principles for the chemical Gibbs function, Helmholtz function, and internal energy. These principles provide a comprehensive theoretical framework for describing fully coupled thermo-mechanicalchemical problems. Konica and Sain (2020) have indeed developed a thermodynamically consistent continuum model that addresses the high-temperature oxidation of polymers, incorporating the complex coupling between diffusion, chemical reactions, and large deformation of polymers. In the context of mechano-thermo-electro-chemical coupling, Yu and Shen (2014) proposed the variational principle of the fully coupled thermal electrical chemical mechanical problem based on irreversible thermodynamics, and derived the fully coupled governing equations including heat conduction, mass diffusion, electrochemical reaction, and electrostatic potential, which can be used to deal with the coupling problem in solids. Suo and Shen (2013b) also established the non-Fick diffusion and stress coupling equations under one-dimensional conditions, and derived approximate analytical solutions for concentration, stress, and displacement using the Laplace transform and the inverse Laplace transform. Considering the microscopic time and chemomechanical coupling effect, Shen (2022) introduced the second-order rate and characteristic time through Taylor expansion to describe the transient process and derived the transient Reynolds transport theorem. Based on the conservation laws, the transient field equations, including mechanical and chemical contributions and microscopic time, were derived, providing a more accurate theoretical framework for studying transient phenomena in complex material systems.

The transient continuum mechano-chemical coupling theory naturally derives finite-speed diffusion equations from conservation laws by introducing characteristic time and second-order rate terms, overcoming the empirical parameter dependence limitation of non-Fick diffusion models. Its core advantages lie in multi-physical field coupling capability and physical self-consistency at microscopic time scales. The objective of our work is to quantitatively investigate the influence of characteristic time on mechano-chemical coupling theory, with systematic comparisons to both classical Fick diffusion and non-Fick diffusion models. The structure of this paper is organized as follows: in Section 2, we introduce the transient continuum chemo-mechanical coupling theory and establish a chemo-diffusion coupling model for lithium ions in a spherical structure. Section 3 discusses the effects of characteristic time and boundary concentration. Finally, we present our conclusions in Section 4.

2. Transient continuum chemo-mechanical coupling theory

By applying the axioms of biomechanics to the transient chemo-mechanical coupling process, and excluding chemical reactions, the mass conservation equation and momentum conservation equation can be derived as follows (Shen, 2022):

$$\frac{\partial c_N}{\partial t} + \frac{t_c}{2} \frac{\partial^2 c_N}{\partial t^2} + \nabla \mathbf{J_N} = 0, \qquad \frac{\partial \rho \mathbf{v}}{\partial t} + \frac{t_c}{2} \frac{\partial^2 \rho \mathbf{v}}{\partial t^2} = \nabla \left(\mathbf{\sigma} - \mathbf{\sigma^V} \right) + \mathbf{b}, \tag{2.1}$$

where c_N is the particle concentration of particle N, t_c is the characteristic time, $\mathbf{J_N}$ is the particle diffusion flux of particle N, ρ is the system density, \mathbf{v} is the velocity, \mathbf{b} is the body force, $\boldsymbol{\sigma}$ is the Cauchy stress, and $\boldsymbol{\sigma^V}$ is the residual stress caused by convective diffusion or chemical reaction, and its expression is

$$\sigma_{ik}^{V} = \left(\rho v_i + t_c \frac{\partial \rho v_i}{\partial t}\right) v_k. \tag{2.2}$$

If the characteristic time t_c is taken as 0 and the convective diffusion of particles is not considered, the above control equations become the classical mass conservation equation and mechanical momentum conservation equation:

$$\frac{\partial c_N}{\partial t} + \nabla \mathbf{J_N} = 0, \qquad \frac{\partial \rho \mathbf{v}}{\partial t} = \nabla \sigma + \mathbf{b}. \tag{2.3}$$

The spherical structure with radius r_0 is shown in Fig. 1. And in this manuscript, the lithium ions are assumed to diffuse inside the spherical structure.

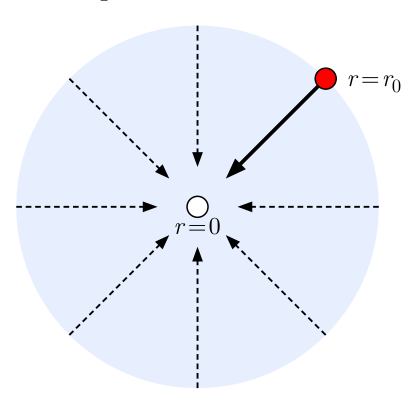


Fig. 1. Schematic diagram of the spherical diffusion model.

Under the influence of concentration, diffusion-induced strain will occur within the sphere. According to Li (1978), the diffusion-induced strain can be expressed as

$$\varepsilon = \Omega(c - c_0),\tag{2.4}$$

where Ω represents the partial molar volume of the sphere, and c_0 represents the initial concentration within the sphere.

Assuming that the deformation in the sphere is relatively small and elastically linear, the material of the spherical model is isotropic, and ions diffuse only radially within the sphere (Suo et al., 2021; 2024). Additionally, the sphere only experiences radial and hoop stresses during ion diffusion, with no shear stress. In a spherical coordinate system, the strain can be expressed in terms of displacement as follows:

$$\varepsilon_r = \frac{\partial u}{\partial r}, \qquad \varepsilon_\theta = \frac{u}{r}.$$
 (2.5)

In the above equation, ε_r and ε_θ represent the radial and hoop stresses, respectively, and u is the radial displacement of the sphere.

In spherical coordinates, the constitutive equations for stress and strain under the influence of force-diffusion coupling are given by the following relations (Zhang et al., 2019):

$$\varepsilon_r = \frac{1}{E} \left(\sigma_r - 2\nu \sigma_\theta \right) + \frac{1}{3} \varepsilon, \qquad \varepsilon_\theta = \frac{1}{E} \left[\sigma_\theta - \nu \left(\sigma_\theta + \sigma_r \right) \right] + \frac{1}{3} \varepsilon, \tag{2.6}$$

where σ_r and σ_θ represent the radial and hoop stresses, respectively, while E and ν represent the elastic modulus and Poisson's ratio, respectively.

Assuming that body forces are negligible during the diffusion process, according to Shen (2022), the equilibrium equation is given by:

$$\nabla(\sigma - \sigma^V) = 0. (2.7)$$

Under the influence of stress, the chemical potential of ion diffusion is given by Chu and Lee (1994):

$$\mu = \mu_0 + RT \ln \frac{c}{c_0} - \Omega \sigma_h, \tag{2.8}$$

where $\sigma_h = (\sigma_r + 2\sigma_\theta)/3$ is the hydrostatic pressure.

The velocity v_b of ions during diffusion can be expressed as

$$v_b = -M\nabla\mu = -\frac{D}{c}\frac{\partial c}{\partial r} + \frac{D\Omega}{RT}\frac{\partial \sigma_h}{\partial r},\tag{2.9}$$

M represents the ionic mobility, ∇ is the gradient operator, and D = MRT is the diffusion coefficient of the material.

Thus, the residual stress can be expressed as

$$\sigma^{V} = \rho \left(-\frac{D}{c} \frac{\partial c}{\partial r} + \frac{D\Omega}{RT} \frac{\partial \sigma_{h}}{\partial r} \right)^{2}. \tag{2.10}$$

Due to the assumption that ions diffuse only in the radial direction, residual stress is generated only in the radial direction within the sphere. Therefore, the equilibrium equation in spherical coordinates is

$$\frac{\partial \left(\sigma_r - \sigma^V\right)}{\partial r} + \frac{2}{r} \left(\sigma_r - \sigma^V - \sigma_\theta\right) = 0. \tag{2.11}$$

Assuming the corresponding boundary conditions are

$$u|_{r=0} = 0, \qquad \sigma_r - \sigma^V|_{r=r_0} = 0.$$
 (2.12)

Under the influence of characteristic time and stress, the diffusion flux J can be expressed as

$$J = \left(c + t_c \frac{\partial c}{\partial t}\right) v_k = -D \left(\frac{\partial c}{\partial r} + \frac{t_c}{c} \frac{\partial c}{\partial t} \frac{\partial c}{\partial r} - \frac{c\Omega}{RT} \frac{\partial \sigma_h}{\partial r} - \frac{t_c \Omega}{RT} \frac{\partial c}{\partial t} \frac{\partial \sigma_h}{\partial r}\right). \tag{2.13}$$

When $t_c = 0$, Eq. (2.13) represents the normal force-diffusion coupling flux under normal conditions.

Ions in the diffusion process obey the law of mass conservation. The mechano-diffusion coupling equation in spherical coordinates is given by

$$\frac{t_c}{2}\frac{\partial^2 c}{\partial t^2} + \frac{\partial c}{\partial t} + \frac{1}{r^2}\nabla\left(r^2J\right) = 0. \tag{2.14}$$

Based on the symmetry of the sphere, the diffusion flux at the center of the sphere is 0. Assuming that the concentration on the outer surface of the sphere is constant at c_1 and the initial concentration of ions inside the sphere is constant at c_0 , the boundary and initial conditions are

$$J|_{r=0} = 0,$$
 $c|_{r=r_0} = c_1,$ $c|_{t=0} = c_0,$ $\frac{\partial c}{\partial t}\Big|_{t=0} = 0.$ (2.15)

To facilitate the simulation calculations, these equations are nondimensionalized by introducing the following dimensionless variables:

$$\overline{r} = \frac{r}{r_0}, \qquad \overline{c} = \frac{c}{c_1}, \qquad \overline{u} = \frac{u}{r_0},$$

$$\overline{\sigma}_h = \frac{\Omega \sigma_h}{RT}, \qquad \overline{f} = \frac{\rho D^2}{Er_0^2}, \qquad \overline{q} = \Omega c_0,$$

$$\overline{\sigma}_r = \frac{\Omega \sigma_r}{RT}, \qquad \overline{\sigma}_\theta = \frac{\Omega \sigma_\theta}{RT}, \qquad \overline{t} = \frac{Dt}{r_0^2},$$

$$\overline{\tau} = \frac{Dt_c}{r_0^2}, \qquad \overline{J} = \frac{Jr_0}{Dc_1}.$$
(2.16)

Substituting these dimensionless variables into Eqs. (2.11) and (2.14), the governing equations becomes

$$\frac{\partial^{2}\overline{u}}{\partial \overline{r}^{2}} + \frac{2}{\overline{r}}\frac{\partial\overline{u}}{\partial \overline{r}} - \frac{2\overline{u}}{\overline{r}^{2}} = \frac{(1+v)(1-2v)}{(1-v)} \left(\frac{2\overline{f}}{\overline{c}^{2}}\frac{\partial\overline{c}}{\partial \overline{r}}\frac{\partial^{2}\overline{c}}{\partial \overline{r}^{2}} + \frac{2\overline{f}}{\overline{c}^{2}}\left(\frac{\partial\overline{c}}{\partial \overline{r}}\right)^{2} \frac{\partial\overline{\sigma}_{h}}{\partial \overline{r}} + 2\overline{f}\frac{\partial\overline{\sigma}_{h}}{\partial \overline{r}}\frac{\partial^{2}\overline{\sigma}_{h}}{\partial \overline{r}^{2}} + 2\frac{\overline{f}}{\overline{r}c^{2}}\left(\frac{\partial\overline{c}}{\partial \overline{r}}\right)^{2} + 2\frac{\overline{f}}{\overline{r}}\left(\frac{\partial\overline{\sigma}_{h}}{\partial \overline{r}}\right)^{2} - 2\frac{\overline{f}}{\overline{c}^{3}}\left(\frac{\partial\overline{c}}{\partial \overline{r}}\right)^{3} - 2\frac{\overline{f}}{\overline{c}^{3}}\frac{\partial^{2}\overline{c}}{\partial \overline{r}^{2}}\frac{\partial\overline{\sigma}_{h}}{\partial \overline{r}^{2}} - 2\frac{\overline{f}}{\overline{c}}\frac{\partial\overline{c}}{\partial \overline{r}}\frac{\partial\overline{\sigma}_{h}}{\partial \overline{r}^{2}} - 2\frac{\overline{f}}{\overline{c}^{3}}\frac{\partial\overline{c}}{\partial \overline{r}}\frac{\partial\overline{\sigma}_{h}}{\partial \overline{r}^{2}} + 2\frac{\overline{f}}{\overline{c}^{3}}\frac{\partial\overline{c}}{\partial \overline{r}}\frac{\partial\overline{\sigma}_{h}}{\partial \overline{r}^{2}} - 2\frac{\overline{f}}{\overline{c}^{3}}\frac{\partial\overline{c}}{\partial \overline{r}}\frac{\partial\overline{\sigma}_{h}}{\partial \overline{r}^{2}} + 2\frac{\overline{f}}{\overline{c}^{3}}\frac{\partial\overline{c}}{\partial \overline{r}}\frac{\partial\overline{\sigma}_{h}}{\partial \overline{r}^{2}} - 2\frac{\overline{f}}{\overline{c}^{3}}\frac{\partial\overline{c}}{\partial \overline{r}}\frac{\partial\overline{\sigma}_{h}}{\partial \overline{r}^{2}} + 2\frac{\overline{f}}{\overline{c}^{3}}\frac{\partial\overline{c}}{\partial \overline{r}}\frac{\partial\overline{\sigma}_{h}}{\partial \overline{r}^{2}} - 2\frac{\overline{f}}{\overline{c}^{3}}\frac{\partial\overline{c}}{\partial \overline{r}}\frac{\partial\overline{\sigma}_{h}}{\partial \overline{r}} + 2\frac{\overline{f}}{\overline{c}^{3}}\frac{\partial\overline{c}}{\partial \overline{r}}\frac{\partial\overline{\sigma}_{h}}{\partial \overline{r}^{2}} - 2\frac{\overline{f}}{\overline{c}^{3}}\frac{\partial\overline{c}}{\partial \overline{r}}\frac{\partial\overline{\sigma}_{h}}{\partial \overline{r}} + 2\frac{\overline{f}}{\overline{c}^{3}}\frac{\partial\overline{c}}{\partial \overline{r}}\frac{\partial\overline{\sigma}_{h}}{\partial \overline{r}^{2}} - 2\frac{\overline{f}}{\overline{c}^{3}}\frac{\partial\overline{c}}{\partial \overline{r}}\frac{\partial\overline{\sigma}_{h}}{\partial \overline{r}^{2}} + 2\frac{\overline{f}}{\overline{c}^{3}}\frac{\partial\overline{c}}{\partial \overline{r}}\frac{\partial\overline{\sigma}_{h}}{\partial \overline{r}^{2}} - 2\frac{\overline{f}}{\overline{c}^{3}}\frac{\partial\overline{c}}{\partial \overline{r}}\frac{\partial\overline{\sigma}_{h}}{\partial \overline{r}^{2}} + 2\frac{\overline{f}}{\overline{c}^{3}}\frac{\partial\overline{c}}{\partial \overline{r}}\frac{\partial\overline{\sigma}_{h}}{\partial \overline{r}^{3}} + 2\frac{\overline{f}}{\overline{c}^{3}}\frac{\partial\overline{c}}{\partial \overline{r}}\frac{\partial\overline{\sigma}_{h}}{\partial \overline{r}^{3}} + 2\frac{\overline{f}}{\overline{c}^{3}}\frac{\partial\overline{c}}{\partial \overline{r}}\frac{\partial\overline{\sigma}_{h}}{\partial \overline{r}^{3}} + 2\frac{\overline{f}}{\overline{c}^{3}}\frac{\partial\overline{c}}{\partial \overline{r}}\frac{\partial\overline{\sigma}_{h}}{\partial \overline{r}^{3}}\frac{\partial\overline{c}}{\partial \overline{r}}\frac{\partial\overline{\sigma}_{h}}{\partial \overline{r}^{3}} + 2\frac{\overline{f}}{\overline{c}^{3}}\frac{\partial\overline{c}}{\partial \overline{r}}\frac{\partial\overline{\sigma}_{h}}{\partial \overline{r}^{3}} + 2\frac{\overline{f}}{\overline{c}^{3}}\frac{\partial\overline{c}}{\partial \overline{r}}\frac{\partial\overline{\sigma}_{h}}{\partial \overline{r}^{3}} + 2\frac{\overline{f}}{\overline{c}^{3}}\frac{\partial\overline{c}}{\partial \overline{r}}\frac{\partial\overline{\sigma}_{h}}{\partial \overline{r}^{3}} + 2\frac{\overline{f}}{\overline{c}^{3}}\frac{\partial\overline{c}}{\partial \overline{r}}\frac{\partial\overline{\sigma}_{h}}{\partial \overline{r}^{3}} + 2\frac{\overline{f}}{\overline{c}^{3}}\frac{\partial\overline{\sigma}_{h}}{\partial \overline{r}^{3}} + 2\frac{\overline{f}}{\overline{c}^{3}}\frac{\partial\overline{\sigma}_{h}}{\partial \overline{r}^{3}}\frac{\partial\overline{\sigma}_{h}}{\partial \overline{r}^{3}} + 2\frac{\overline{f}}{\overline{c}^{3}}\frac{\partial\overline{\sigma}_{h}}{\partial \overline{r}^{3}}\frac{\partial\overline{\sigma}_{h}}{\partial \overline{r}^{3}}\frac{\partial\overline$$

$$\frac{\overline{\tau}}{2} \frac{\partial^2 \overline{c}}{\partial \overline{t}^2} + \frac{\partial \overline{c}}{\partial \overline{t}} = \frac{\partial^2 \overline{c}}{\partial \overline{r}^2} - \frac{\overline{\tau}}{\overline{c}^2} \frac{\partial \overline{c}}{\partial \overline{t}} \left(\frac{\partial \overline{c}}{\partial \overline{r}} \right)^2 + \frac{\overline{\tau}}{\overline{c}} \frac{\partial^2 \overline{c}}{\partial \overline{t} \partial \overline{r}} \frac{\partial \overline{c}}{\partial \overline{r}} + \frac{\overline{\tau}}{\overline{c}} \frac{\partial \overline{c}}{\partial \overline{t}} \frac{\partial^2 \overline{c}}{\partial \overline{r}^2} - \frac{\partial \overline{c}}{\partial \overline{r}} \frac{\partial \overline{\sigma}_h}{\partial \overline{r}} - \overline{c} \frac{\partial^2 \overline{\sigma}_h}{\partial \overline{r}^2} \\
- \overline{\tau} \frac{\partial^2 \overline{c}}{\partial \overline{t} \partial \overline{r}} \frac{\partial \overline{\sigma}_h}{\partial \overline{r}} - \overline{\tau} \frac{\partial \overline{c}}{\partial \overline{t}} \frac{\partial^2 \overline{\sigma}_h}{\partial \overline{r}^2} + \frac{2}{\overline{c}} \left(\frac{\partial \overline{c}}{\partial \overline{r}} + \frac{\overline{\tau}}{\overline{c}} \frac{\partial \overline{c}}{\partial \overline{t}} \frac{\partial \overline{c}}{\partial \overline{r}} - \overline{c} \frac{\partial \overline{\sigma}_h}{\partial \overline{r}} - \overline{\tau} \frac{\partial \overline{c}}{\partial \overline{t}} \frac{\partial \overline{\sigma}_h}{\partial \overline{r}} \right). (2.18)$$

The corresponding initial and boundary conditions are

$$\overline{u}|_{\overline{r}=0} = 0, \qquad \overline{\sigma}_r - \overline{\sigma}^V|_{\overline{r}=1} = 0, \qquad \overline{J}|_{\overline{r}=0} = 0,
\overline{c}|_{\overline{r}=1} = 1, \qquad \overline{c}|_{\overline{t}=0} = \frac{31}{33}, \qquad \frac{\partial \overline{c}}{\partial \overline{t}}|_{\overline{t}=0} = 0.$$
(2.19)

3. Results and discussion

The primary computational methods for mechanical-chemical coupling problems are the finite element method (Chen et al., 2017), phase field modeling (Chen, 2002), and using COMSOL software (Li et al., 2024). In this paper, we use COMSOL Multiphysics field coupling simulation software to compute the partial differential equations directly. The partial differential equation (PDE) module in COMSOL Multiphysics was used to conduct the simulation study. The mesh was processed using extreme refinement, dividing it into 100 cells with a maximum size

of 1.5×10^{-9} . A transient study was added, with output time steps set at $0.1 \,\mathrm{s}$ and a total calculation duration of 6 s. The convergence tolerance was adjusted to 1×10^{-7} to ensure simulation accuracy, and the simulation was executed to obtain the numerical results. Table 1 shows the parameter settings for the simulation calculations.

Parameter	Symbol	Values
Elastic modulus [GPa]	E	10
Diffusion coefficient [m ² /s]	D	6.8×10^{-16}
Partial molar volume [m ³ /mol]	Ω	3.497×10^{-6}
Poisson's ratio	ν	0.27
Particle radius [m]	r_0	1.5×10^{-7}
Initial concentration [mol/m ³]	c_0	310
Boundary concentration [mol/m ³]	c_1	330
Gas constant $[J/(mol \cdot K)]$	R	8.314
Absolute temperature [K]	T	300
Characteristic time [s]	t_c	0.6
Density [kg/m ³]	ρ	2000

Table 1. Material parameters.

To compare the changes in concentration and stress during the diffusion process under different diffusion forms, a coefficient k_s is introduced in front of the additional terms in Eqs. (2.11) and (2.13). The modified equations are

$$\frac{\partial \left(\sigma_r - k_s \sigma^V\right)}{\partial r} + \frac{2}{r} \left(\sigma_r - k_s \sigma^V - \sigma_\theta\right) = 0, \qquad J = \left(c + k_s t_c \frac{\partial c}{\partial t}\right) v_k, \tag{3.1}$$

 k_s is 1 for the theoretical model used in this paper and k_s is 0 for the theoretical model used for non-Fick diffusion, the difference between the two theories can be clearly seen through the equation. If no special instructions are given, k_s takes 1.

Figure 2 presents a comparison of concentration, displacement, radial stress, and hoop stress between the non-Fick diffusion theory (non-Fick, $k_s = 0$) and the mechano-diffusion coupling model proposed in this section (our model, $k_s = 1$) at a characteristic time value of $\bar{\tau} = 1.8 \times 10^{-2}$ ($t_c = 0.6 \, \mathrm{s}$). Ions are seen to progressively spread from the edge towards the center in Fig. 2a. When $k_s = 0$ and $k_s = 1$, the concentration changes abruptly before diffusion reaches the sphere's center. There are no abrupt variations in concentration for either model after diffusion reaches the sphere's center ($\bar{t} = 0.18$), and the concentration variations along the radial direction are similar. At the same position, the ion concentration increases with increasing diffusion time, and the ion concentration under our model is higher than that under the non-Fick diffusion model. This is because the presence of characteristic time in our model leads to an increase in the ion diffusion flux, which in turn results in a higher ion concentration over a specific period of time. The spherical model's displacement diagram is shown in Fig. 2b. The graphic demonstrates that ion diffusion causes displacement within the sphere. At the same moment, the radial displacement in our model is greater than that in the non-Fick diffusion model due to ion diffusion.

It is evident from Fig. 2c that the radial stress rises with proximity to the sphere's center. In our model, the radial stress in the region reached by ion diffusion is lower than that under non-Fick diffusion at the same time and location. This is because, within the same time frame, the increase in diffusion flux leads to a higher ion concentration and greater displacement within our model. According to the formula for radial stress, an increase in displacement leads to an increase in radial stress, while an increase in concentration leads to a decrease in radial

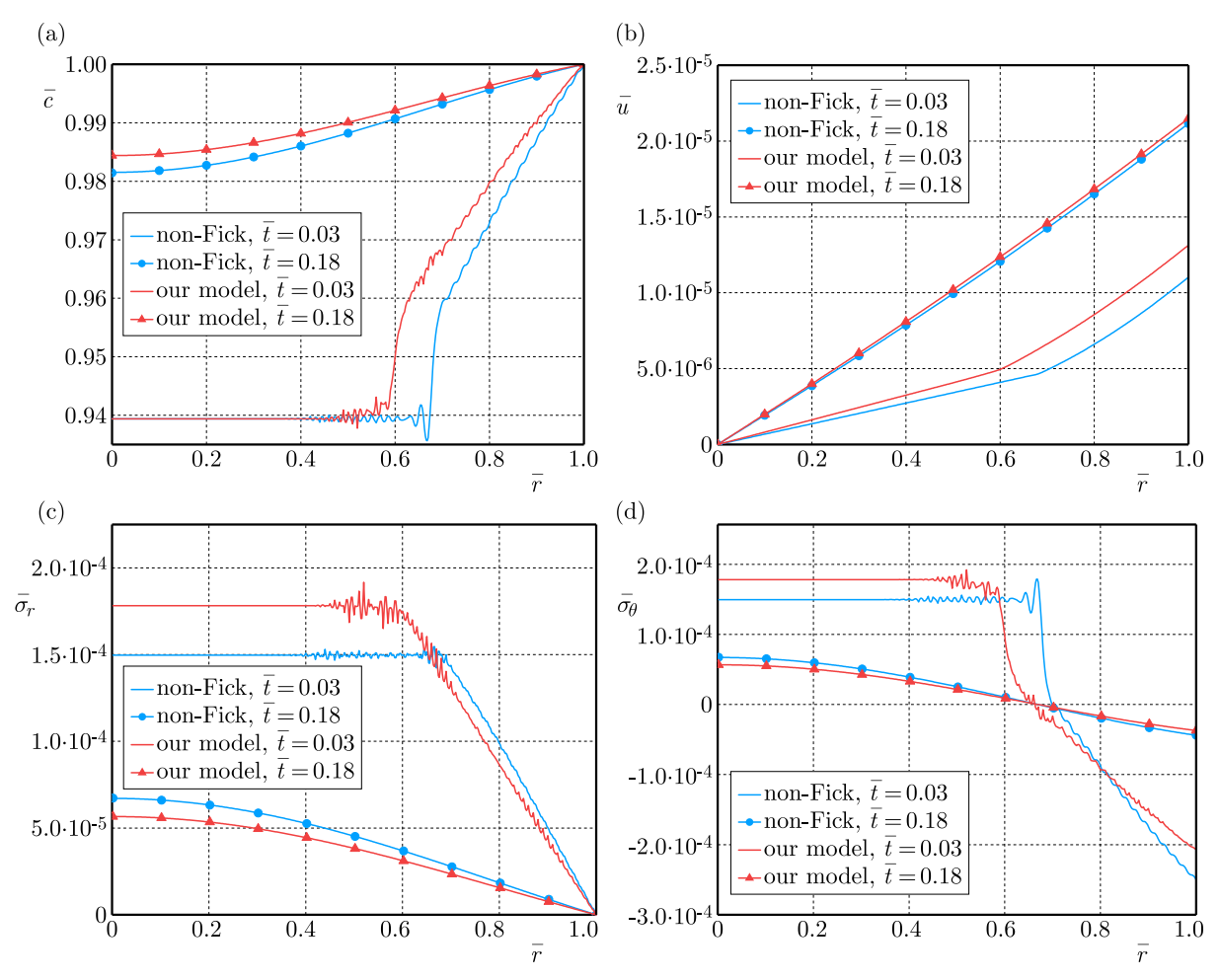


Fig. 2. Comparison of concentration (a); displacement (b); radial stress (c); and hoop stress (d) between non-Fick diffusion and our model.

stress. However, the effect of displacement on radial stress is less significant than the effect of concentration on radial stress. Therefore, in our mechanic-diffusion coupling model, the radial stress is less than that in the non-Fick mechano-diffusion coupling model. In regions where ions have not diffused, the concentration remains unchanged, and radial stress is influenced solely by the changes in displacement. Since both the displacement and its gradient are greater in our model compared to the non-Fick diffusion model, in areas where the concentration has not changed at the same moment, the radial stress in our model is greater than that in the non-Fick diffusion model. From Fig. 2d, it can be observed that in both scenarios, the hoop stress is compressive near the outer surface and tensile near the center of the sphere. As the ion moves from the outer surface towards the center, the magnitude of the hoop stress first decreases to zero and then gradually increases. In the regions where ions have not diffused, the hoop stress in our model is greater than that in the non-Fick diffusion model. At $\bar{t}=0.18$, within the sphere at the same moment, the hoop stress in our model is less than that under both non-Fick and Fick diffusion, for the same reasons as with the radial stress.

Figure 3 illustrates the distribution of ion concentration, displacement, radial stress, and hoop stress within the model at different times for a characteristic time of $\bar{\tau} = 1.8 \times 10^{-2}$ (0.6 s). From Fig. 3a, it can be observed that during the diffusion process, ions diffuse from the outer surface of the sphere towards the center. Moreover, as indicated by the blue, green, and red curves, there is no change in ion concentration near the center during the period when ions have not yet diffused to that area. This is due to the fact that in our model, the diffusion speed of ions is not infinite; ions diffuse at a finite speed. When concentration boundary conditions

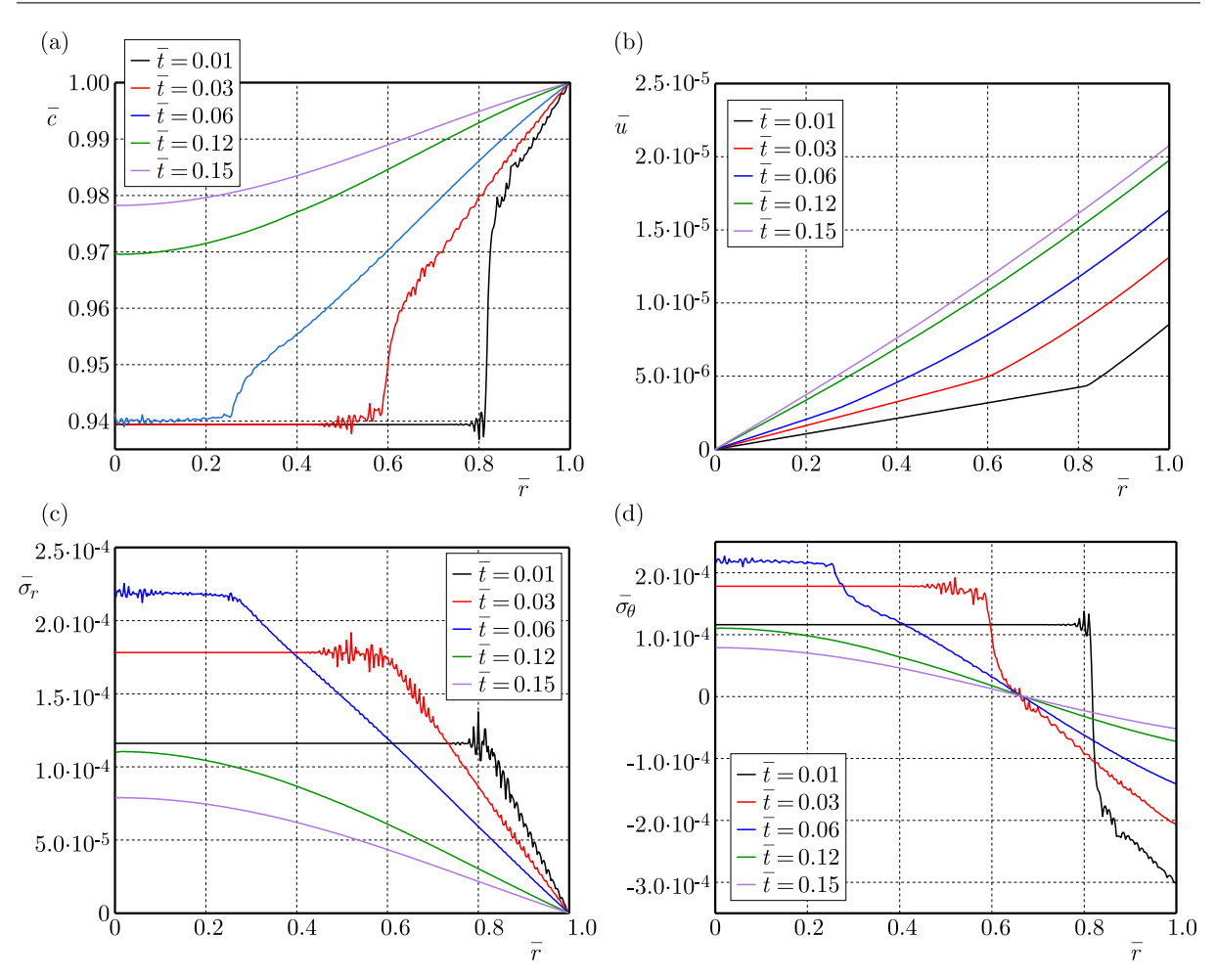


Fig. 3. Distribution of concentration (a); displacement (b); radial stress (c); and hoop stress (d) at different diffusion times.

are applied, the ion concentration within the model does not change immediately but senses the change after a specific period. Furthermore, within a specific time frame, the influence of the second-order terms causes the concentration diffusion curves to exhibit oscillatory behavior. After a period of time, as the impact of the second-order terms diminishes, the oscillatory nature of the curves disappears. It is evident from Fig. 3b, which displays the displacement, that the model's displacement rises as the diffusion time does. Before the diffuse reaches the center of the sphere, at three time points $\bar{t}=0.01, \bar{t}=0.03,$ and $\bar{t}=0.06,$ it can be seen that in the region where the concentration has not changed, the model's displacement maintains a linear change. This also confirms the reason why the radial stress and hoop stress in the region where the concentration has not changed remain constant.

It is evident from Fig. 3c that the model's radial stress is tensile and increases gradually from the outer surface towards the center of the sphere in the region where ions have diffused. When $\bar{t}=0.01$, $\bar{t}=0.03$, and $\bar{t}=0.06$, in the regions where ions have not diffused, the radial stress remains constant, while in the regions where ions have diffused, the radial stress shows a decreasing trend with increasing time. According to the formula, the radial stress is determined by the ion concentration and displacement. An increase in concentration leads to a decrease in radial stress, while an increase in displacement leads to an increase in radial stress. In the region where ions have diffused, as the diffusion time increases, the concentration change at the same position becomes greater. The effect of concentration change on radial stress is more significant than that of displacement change. Therefore, in the region where ions have diffused, the radial stress decreases with increasing time. In the regions where ions have not diffused (the platform

parts of the red, blue, and black solid lines), the concentration remains unchanged, and the radial stress is only affected by the changes in displacement. At this time, the radial stress decreases with the increase in time. It is shown by Fig. 3d that the hoop stress of the model is compressive at the outer surface and tensile at the center of the sphere. In the region where ions have diffused, the hoop stress decreases from the outer surface towards the center, reaching zero before gradually increasing. The hoop stress also decreases over time. From Fig. 3d, at the time points $\bar{t}=0.01, \bar{t}=0.03,$ and $\bar{t}=0.06,$ it can be seen that in the regions where ions have not diffused, the hoop stress remains unchanged.

From Figs. 4a and 4b, it can be observed that the ion concentration and displacement within the model increase with the increase in characteristic time. The characteristic time affects the ion diffusion flux, which in turn increases with the characteristic time. Therefore, within the same time frame, the higher the characteristic time, the higher the ion concentration.

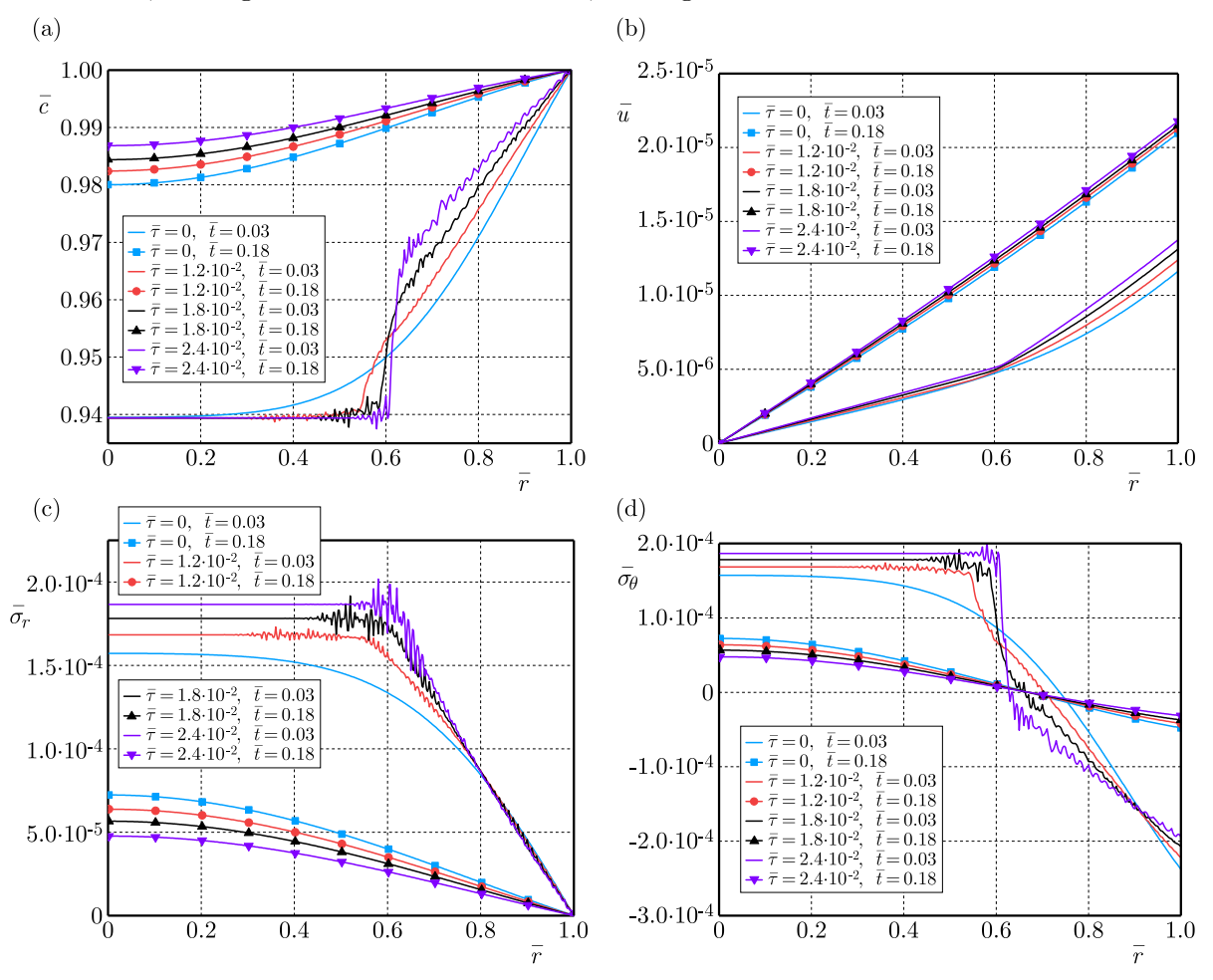


Fig. 4. Distribution of concentration (a); displacement (b); radial stress (c); and hoop stress (d) under different characteristic times.

According to Figs. 4c and 4d, at $\bar{t}=0.03$ ($t=1\,\mathrm{s}$, no graphic line) in the regions where ions have not diffused, both radial stress and hoop stress increase with the increase in characteristic time. This is because the displacement within the model increases with characteristic time, and when the concentration remains unchanged, both radial stress and hoop stress increase with the increase in displacement. After the ions have diffused to the center of the sphere ($\bar{t}=0.18$, graphic line), both radial stress and hoop stress within the model decrease with the increase in characteristic time. This is because both radial stress and hoop stress are determined by changes in displacement and concentration, with the impact of concentration changes on radial and hoop stress being greater than the effects produced by changes in displacement. As the concentration

change increases with the increase in characteristic time, in the curve at $\bar{t} = 0.18$, the radial stress and hoop stress decrease with the increase in characteristic time.

4. Conclusion

Based on the theory of transient mechano-chemical coupling, this paper investigates the mechano-chemical coupled diffusion processes of ions within a spherical structure, exploring the effects of characteristic time and boundary concentration on the distribution of concentration, displacement, radial stress, and hoop stress within the structure. The results indicate that:

- 1) The presence of characteristic time transforms the classical chemical diffusion control equation from a parabolic type to a hyperbolic type, changing the diffusion speed from infinite to finite. Concentration curves exhibit oscillatory behavior. Consequently, the concentration, stress, and displacement curves distinctly show two regions: the area that has been diffused and the area that has not been diffused. At the interface between these two regions, there is a sudden change in the concentration and stress curves.
- 2) The characteristic time influences the magnitude of ion concentration, displacement, radial stress, and hoop stress. Ion concentration and displacement increase with the increase in characteristic time. Radial stress and hoop stress increase in regions where ions have not yet diffused with the increase in characteristic time, while they decrease in regions where ions have already diffused with the increase in characteristic time.

Acknowledgments

This work was supported by the National Natural Science Foundation of China (grant no. 12272095 and 12402212).

References

- Chen, J.Y., Wang, H.L., Yu, P.F., & Shen, S.P. (2017). A finite element implementation of a fully coupled mechanical-chemical theory. *International Journal of Applied Mechanics*, 9(3), Article 1750040. https://doi.org/10.1142/s1758825117500405
- 2. Chen, L.Q. (2002). Phase-field models for microstructure evolution. *Annual Review of Materials Research*, 32, 113–140. https://doi.org/10.1146/annurev.matsci.32.112001.132041
- 3. Chen, X.Q., Deng, F., & Shen, S.P. (2023). Chemomechanical finite element analysis for surface oxidation of Aluminum alloy. *Acta Mechanica*, 234(4), 1713-1732. https://doi.org/10.1007/s00707-022-03463-5
- 4. Chu, J.L., & Lee, S.B. (1994). The effect of chemical stress on diffusion. Journal of Applied Physics, 75(6), 2823-2829. https://doi.org/10.1063/1.356174
- 5. Dai, L., & Xiao, R. (2021). A thermodynamic-consistent model for the thermo-chemo-mechanical couplings in amorphous shape-memory polymers. *International Journal of Applied Mechanics*, 13(2), Article 2150022. https://doi.org/10.1142/s1758825121500228
- 6. Dong, H.X., & Jiang, R.Q. (1995). Theoretical study of mass transfer behavior in transient mass transfer process (in Chinese). *Journal of Harbin Engineering University*, 16(3), 88–94.
- Hu, H., Yu, P.F., & Suo, Y.H. (2020). Stress induced by diffusion and local chemical reaction in spherical composition-gradient electrodes. Acta Mechanica, 231(7), 2669–2678. https://doi.org/10.1007/s00707-020-02652-4
- 8. Hu, S., & Shen, S. (2013). Non-equilibrium thermodynamics and variational principles for fully coupled thermal-mechanical-chemical processes. *Acta Mechanica*, 224 (12), 2895–2910. https://doi.org/10.1007/s00707-013-0907-1

- Konica, S., & Sain, T. (2020). A thermodynamically consistent chemo-mechanically coupled large deformation model for polymer oxidation. *Journal of the Mechanics and Physics of Solids*, 137, Article 103858. https://doi.org/10.1016/j.jmps.2019.103858
- 10. Kuang, Z.B. (2014). Discussions on the temperature wave equation. *International Journal of Heat and Mass Transfer*, 71, 424–430. https://doi.org/10.1016/j.ijheatmasstransfer.2013.12.016
- 11. Li, J.C.M. (1978). Physical chemistry of some microstructural phenomena. *Metallurgical and Materials Transactions A*, 9(10), 1353–1380. https://doi.org/10.1007/BF02661808
- 12. Li, X., Gao, J., Zhou, W., & Li, H. (2024). Application of COMSOL multiphysics in lithium-ion batteries (in Chinese). *Energy Storage Science and Technology*, 13(2), 546–567.
- 13. Liu, K.C. (2007). Simultaneous estimation of relaxation time and diffusion coefficient during the rapid transient mass transfer. *Journal of the Chinese Society of Mechanical Engineers*, 28(5), 541–547. https://doi.org/10.29979/JCSME.200710.0009
- Nguyen, T.T., Waldmann, D., & Bui, T.Q. (2019). Computational chemo-thermo-mechanical coupling phase-field model for complex fracture induced by early-age shrinkage and hydration heat in cement-based materials. Computer Methods in Applied Mechanics and Engineering, 348, 1–28. https://doi.org/10.1016/j.cma.2019.01.012
- 15. Shen, S.P. (2022). Transient continuum mechanics and chemomechanics. *Journal of Applied Mechanics*, 89(6), Article 061004. https://doi.org/10.1115/1.4054061
- Suo, Y.H., Hu, H., & Liu, J. (2021). Fully chemo-mechanical coupling analysis of a spherical electrode with reversible chemical reaction. *International Journal of Energy Research*, 45(6), 9667–9676. https://doi.org/10.1002/er.6430
- 17. Suo, Y.H., & Shen, S.P. (2013a). Analytical solution for 2D non-Fickian transient mass transfer with arbitrary initial and periodic boundary conditions. *ASME Journal of Heat and Mass Transfer*, 135(8), Article 082001. https://doi.org/10.1115/1.4024352
- 18. Suo, Y.H., & Shen, S.P. (2013b). Analytical solution for one-dimensional coupled non-Fick diffusion and mechanics. *Archive of Applied Mechanics*, 83(3), 397–411. https://doi.org/10.1007/s00419-012-0687-4
- Suo, Y.H., Yang, H., & Jia, Q.N. (2024). Coupled diffusion-mechanical analysis with dislocation effect in porous spherical electrode. Solid State Ionics, 404, Article 116422. https://doi.org/10.1016/ j.ssi.2023.116422
- 20. Yan, G.S., Wu, Y.H., Liu, W.Y., Yu, W.S., & Shen, S.P. (2024). Stress evolution in enamel coating/Ni-based alloy systems during isothermal oxidation. *Journal of Applied Physics*, 135(8), Article 085103. https://doi.org/10.1063/5.0185084
- 21. Yu, P.F., Hu, S.L., & Shen, S.P. (2016). Electrochemomechanics with flexoelectricity and modelling of electrochemical strain microscopy in mixed ionic-electronic conductors. *Journal of Applied Physics*, 120(6), Article 065102. https://doi.org/10.1063/1.4960445
- 22. Yu, P.F., & Shen, S.P. (2014). A fully coupled theory and variational principle for thermal-electrical-chemical-mechanical processes. *Journal of Applied Mechanics*, 81(11), Article 111005. https://doi.org/10.1115/1.4028529
- 23. Zhang, K., Li, Y., Wang, F., Zheng, B.L., & Yang, F.Q. (2019). A phase-field study of the effect of local deformation velocity on lithiation-induced stress in wire-like structures. *Journal of Physics D: Applied Physics*, 52(14), Article 145501. https://doi.org/10.1088/1361-6463/ab00dc